

RIS-Empowered Non-Linear Energy Harvesting Communications Over Nakagami- m Channels

Hakan Alakoca¹, Graduate Student Member, IEEE, Mohammadreza Babaei², Student Member, IEEE, Lutfiye Durak-Ata³, Senior Member, IEEE, and Ertugrul Basar⁴, Senior Member, IEEE

Abstract—We propose novel reconfigurable-intelligent-surface (RIS)-based energy harvesting (EH) systems with linear EH (L-EH) and non-linear EH (NL-EH) models where channels are exposed to Nakagami- m fading. We also compare two RIS-based EH systems in terms of RIS locations, namely RIS-EH and RIS-information processing (RIS-IP). In the RIS-EH, RIS increases the amount of harvested energy, while in the RIS-IP, RIS is utilized to improve the information processing link. Closed-formed expressions of throughput, outage probability, and average harvested power are derived and confirmed via simulation. The L-EH model overestimates system performance, while the NL-EH model provides a realistic interpretation of EH system design.

Index Terms—Average harvested power, energy harvesting, outage probability, reconfigurable intelligent surfaces.

I. INTRODUCTION

GREEN communications promise to enable sustainability, energy efficiency, and high reliability in next-generation wireless networks. Energy harvesting (EH) with wireless power transfer (WPT) is an advanced technique that significantly reduces the energy consumption of wireless devices [1]. Besides, reconfigurable intelligent surfaces (RIS) have attracted significant attention in academia and industry and are revolutionizing the smart radio environment concept by changing the electromagnetic behavior of transmitted signals. Joint usage of RIS and EH techniques is promising for green communications, comprising opportunities for improvement.

An RIS-based EH system is presented in [2] to increase physical layer security where the channels are exposed to Rician fading. In addition, a low-complexity algorithm to solve an average secrecy rate maximization problem is investigated. Studies that examined specific EH-models in RIS-empowered networks are listed as [3]–[6]. An analytical approach is presented in [3] for analyzing the battery recharge time (BRT) in WPT systems with RIS-aided links. According to the results, the mean duration of the BRT may be reduced to one-fourth by increasing the number of RIS components. The outage performance of RIS-assisted wireless powered

multi-user communication networks is investigated in [4] considering round-robin and maximum capacity scheduling based on time switching. According to [5], suboptimal systems for RIS-aided EH networks can generate roughly 80% of the harvested power of an ideal scheme, reducing the system's communication overhead. An RIS-assisted non-linear EH (NL-EH) based wireless communication system is given in [6] with ultra-reliable low-latency communications restrictions for industrial applications. In addition, the impact of several parameters on system performance, such as the number of RIS meta-atoms, blocklength, packet size, and RIS location, are also investigated.

Massive machine-type communication (mMTC) use case aims at being cost-effective with low power consumption and long-time availability communication. To fulfill these demands, we have focused on specific individual two-use cases. In this letter, the performance of an RIS-empowered both linear EH (L-EH) and NL-EH system over Nakagami- m channels is investigated, considering throughput, outage probability, and the average harvested power metrics. The state-of-the-art lacks any analysis of the impact of harvested power on wireless data transmissions in RIS-enabled systems. We diversify and analyze system models with two unique cases, namely, RIS-EH and RIS information processing (RIS-IP), to demonstrate the functionality of RIS on EH systems in a realistic approach. In RIS-EH, RIS aids in increasing the amount of harvested power, which results in a highly transmittable power source. In the latter case, RIS is specialized to boost received signal-to-noise ratio (SNR) at the destination node. Main contributions of this letter are given as follows:

- 1) Throughput and outage probability of a WPT-based and RIS-EH, and RIS-IP network are analytically evaluated, considering both L/NL-EH models to quantify the impact of realistic models on the system performance.
- 2) Performance of RIS-EH and RIS-IP are also compared for varied system parameters for L/NL-EH models.
- 3) The closed-form expressions, which are consistent with numerical simulations of average harvested power analysis of RIS-based EH systems, are derived.

Manuscript received 16 April 2022; revised 23 May 2022; accepted 7 June 2022. Date of publication 13 June 2022; date of current version 11 September 2022. This work was supported in part by the Istanbul Technical University Vodafone Future Lab under Project ITUVF20180701P09. The work of Ertugrul Basar is supported by TUBITAK 120E401 project. The associate editor coordinating the review of this letter and approving it for publication was L. Mohjazi. (Corresponding author: Hakan Alakoca.)

Hakan Alakoca, Mohammadreza Babaei, and Lutfiye Durak-Ata are with the Information and Communications Research Group, Informatics Institute, Istanbul Technical University, 34469 Istanbul, Turkey (e-mail: alakoca@itu.edu.tr; babaei@itu.edu.tr; durakata@itu.edu.tr).

Ertugrul Basar is with the Communications Research and Innovation Laboratory (CoreLab), Department of Electrical and Electronics Engineering, Koç University, 34450 Istanbul, Turkey (e-mail: ebasar@ku.edu.tr).

Digital Object Identifier 10.1109/LCOMM.2022.3182482

Notations: Statistical expectation and the absolute value is denoted by $\mathbb{E}[\cdot]$ and $|\cdot|$, respectively. Modified Bessel function of first kind [7, 8.406] is indicated as $I_\nu(\cdot)$ with order ν . $\Gamma(\cdot)$ denotes as Gamma function [7, 6.41]. Confluent hyper-geometric function of the second kind is represented as $M_{\nu, \mu}(\cdot)$ [7, 9.22]. In addition, $G_{p, q}^{m, n}(\cdot)$ is defined as the Meijer-G-function [7, 9.30]. Moreover, $G_{q, p}^{n, m; m_1, n_1; m_2, n_2}(\cdot)$ denotes the Bivariate Meijer-G function [8, 07.34.21.0081.01]. Furthermore, $Q(\cdot, \cdot)$ is referred as generalized Marcum-Q function [9, 2.3-36]. In addition, $Q(\cdot)$ is represented as Gaussian-Q function [9, 2.3-10]. $\text{erfc}(\cdot)$ is given as complementary error function [9, 2.3-17]. $f(\cdot)$ and $F(\cdot)$ represents PDF and CDF, respectively. $\bar{F}(\cdot)$ denotes complimentary CDF of $F(\cdot)$.

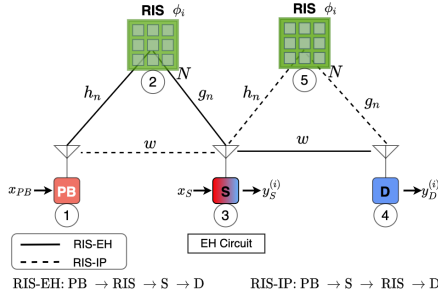


Fig. 1. The proposed system model based on RIS-relayed EH networks.

II. SYSTEM MODEL

An WPT-based proposed system for two individual EH operations with the aid of an RIS is depicted in Fig. 1. The communication environment consists of a power beacon (PB) transmitter node, an RIS by N surface components, source (S) node, and destination (D) node. Also, PB, S, and D are equipped with single antenna. Please also note that equipping multiple antennas for PB and S is beyond the scope of this work due to its mathematical complexity. Instead, we prefer to utilize SISO to obtain an analytical solution, which is suitable for cost-effective mMTC for Internet-of-Things (IoT) devices. Besides, the system model divided into two individual cases to investigate impact of relaying position of RIS. In the RIS-EH case, RIS node is operating as transferring energy bearing signal from PB \rightarrow S. Next, in the RIS-IP case, RIS equipment is used as IP relaying procedure from S \rightarrow D. Also, it is noted that signaling routes follows PB \rightarrow RIS \rightarrow S \rightarrow D and PB \rightarrow S \rightarrow RIS \rightarrow D links, for RIS-EH and RIS-IP cases, respectively. For direct links, w is denoted as channels between S \rightarrow D, and PB \rightarrow S for RIS-EH and RIS-IP cases, respectively. For RIS-relaying, PB \rightarrow RIS and PB \rightarrow S links represented as h_n while RIS \rightarrow S and RIS \rightarrow D links denoted as g_n for the n -th surface element of RIS. All the channels are exposed to the Nakagami- m fading.

The use of PIN diodes allows each surface element to tune electromagnetic phase shifts. In addition, PIN diodes change their status according to channel state information (CSI) via a microcontroller. Moreover, reconfiguration is operated by using the microcontroller to adjust incident signal and reflect by maximizing received SNR via $\phi_n = -\exp(\phi_{h_n} + \phi_{g_n})$. Here, ϕ_{h_n} and ϕ_{g_n} represents phase of the h_n and g_n , respectively. The received signal at the first time slot of $T/2$ at the S for each individual cases can be expressed as

$$y_S^{(i)} = \sqrt{P_B L_{PB \rightarrow S}^{(i)}} \beta^{(i)} x_{PB} + n_S, \quad (1)$$

where P_B is the transmit power of the PB,

$L_{PB \rightarrow S}^{(i)}$ represent path-loss of the PB \rightarrow S. Please note that $i = \{1, 2\}$ denotes RIS-EH and RIS-IP cases, respectively. $L_{PB \rightarrow S}^{(1)} = 1/(d_{12}d_{23})^v$, and $L_{PB \rightarrow S}^{(2)} = 1/d_{13}^v$ where d_{xy} represents the distance between $x \rightarrow y$ nodes, and $\{x, y\} \in \{1, 2, 3, 4, 5\}$. Moreover, v is denoted as path-loss coefficient. Here, $\beta^{(1)} = \zeta$, and $\beta^{(2)} = w$ with distributions $\zeta \sim \mathcal{N}(\mu, \sigma^2)$, and $w \sim \text{Gamma}(m_w, \Omega_w)$, respectively, where $\zeta = \sum_{n=1}^N h_n \phi_n g_n$. Moreover, $\mu = N\mathcal{A}$ and $\sigma^2 = N(\Omega_h \Omega_g - \mathcal{A}^2)$ where $\mathcal{A} = \sqrt{\frac{\Omega_h \Omega_g}{m_h m_g} \frac{\Gamma(m_h + 0.5) \Gamma(m_g + 0.5)}{\Gamma(m_h) \Gamma(m_g)}}$. Here, m_j and $\Omega_j = \mathbb{E}[|\beta^{(i)}|^2]$ are the Nakagami- m channel parameter,

and the channel gain, respectively, where $j \in \{w, h_n, g_n\}$. In addition, n_S represents complex Gaussian noise component with zero mean and σ_S^2 variance and x_{PB} is the energy bearing signal. The harvested energy at S can be calculated as $E_H^{(i)} = \eta T \mathbb{E}[|y_S^{(i)}|^2]/2$ where η is denoted as energy conversion efficiency, and $\mathbb{E}[|y_S^{(i)}|^2] = P_B L_{PB \rightarrow S}^{(i)} |\beta^{(i)}|^2$. Please note that, the noise power is neglected as in [10]. Moreover, the harvested power is calculated as $P_S^{(i)} = 2E_H^{(i)}/T$.

For simplicity, we define $P_S^{L(i)}$, and $P_S^{NL(i)}$ as the transmit power of S for L-EH and piece-wise NL-EH models, respectively, and is given as

$$P_S^{(i)} \rightarrow \begin{cases} P_S^{L(i)} = \mathcal{U}^{(i)}, \\ P_S^{NL(i)} = \begin{cases} 0, & \mathcal{U}^{(i)} \leq P_m, \\ \mathcal{U}^{(i)}, & P_m \leq \mathcal{U}^{(i)} \leq P_{th}, \\ P_{th}, & \mathcal{U}^{(i)} > P_{th}, \end{cases} \end{cases} \quad (2)$$

where $\mathcal{U}^{(i)} = P_S^{(i)} = \rho^{(i)} |\beta^{(i)}|^2$ and $\rho^{(i)} = \eta P_B L_{PB \rightarrow S}^{(i)}$. Here, P_m and P_{th} are the sensitivity and saturation threshold level of energy constrained node S. Please note that P_m guarantees a minimum power to control signaling, resource allocation, and signal transmission. In the second time slot of $T/2$ duration, the received signal at D is given as

$$y_D^{(i)} = \sqrt{P_S^{(i)} L_{S \rightarrow D}^{(i)}} \Upsilon^{(i)} x_S + n_D, \quad (3)$$

where $L_{S \rightarrow D}^{(i)}$ denotes path loss component of the S \rightarrow D link in which $L_{S \rightarrow D}^{(1)} = 1/d_{34}^v$, $L_{S \rightarrow D}^{(2)} = 1/(d_{35}d_{54})^v$. Moreover, n_D represents the circularly symmetric Gaussian noise component at D with zero mean and σ_D^2 variance. Besides, x_S is the transmitted signal of S. Here, $\Upsilon^{(1)} = w$, and $\Upsilon^{(2)} = \zeta$. Considering (3), received SNR at D for both the L-EH and NL-EH models as well as RIS-EH and RIS-IP cases is expressed as,

$$\gamma_D^{(i)} \rightarrow \begin{cases} \gamma_D^{L(i)} = \mathcal{U}^{(i)} \mathcal{V}^{(i)}, \\ \gamma_D^{NL(i)} = \begin{cases} 0, & \mathcal{U}^{(i)} \leq P_m, \\ \mathcal{U}^{(i)} \mathcal{V}^{(i)}, & P_m \leq \mathcal{U}^{(i)} \leq P_{th}, \\ P_{th} \mathcal{V}^{(i)}, & \mathcal{U}^{(i)} > P_{th}, \end{cases} \end{cases} \quad (4)$$

where $\mathcal{V}^{(i)} = v^{(i)} |\Upsilon^{(i)}|^2$ and $v^{(i)} = L_{S \rightarrow D}^{(i)} / \sigma_D^2$. For simplicity, it is assumed that $\mathcal{Z} = \zeta^2$ and $\mathcal{X} = w$ where ζ^2 is the non-central chi-square distribution.

The CDF and PDF of the \mathcal{Z} are expressed as [9, 2.3-35],

$$F_{\mathcal{Z}}(z) = 1 - Q_{1/2} \left(\mu/\sigma, \sqrt{z/(\kappa\sigma^2)} \right), \quad (5)$$

and

$$f_{\mathcal{Z}}(z) = \kappa^{-0.75} \alpha z^{-0.25} \exp\left(\frac{-z}{2\sigma^2 \kappa}\right) I_{-0.5} \left(\frac{\mu}{\sigma^2} \sqrt{\frac{z}{\kappa}} \right), \quad (6)$$

where $\alpha = \sqrt{\mu} \exp(-\mu^2/2\sigma^2) / 2\sigma^2$ for $i = 1$ and $i = 2$, $\kappa = \rho^{(1)}$ and $\kappa = v^{(2)}$, respectively. Here, $Q_{1/2}(\varpi_1, \varpi_2) = Q(\varpi_2 - \varpi_1) + Q(\varpi_2 + \varpi_1)$ [11] and $Q(\varpi) = \text{erfc}(\varpi/\sqrt{2})/2$. The CDF and PDF of the \mathcal{X} are given as,

$$F_{\mathcal{X}}(x) = 1 - \exp(-mx/\Omega_w \varepsilon) \sum_{t=0}^{m-1} (mx/\Omega_w \varepsilon)^t / t!, \quad (7)$$

and

$$f_{\mathcal{X}}(x) = m^m x^{m-1} \exp(-mx/\Omega_w \varepsilon) / ((\Omega_w \varepsilon)^m \Gamma(m)), \quad (8)$$

where for $i = 1$ and $i = 2$ cases, $\varepsilon = v^{(1)}$ and $\varepsilon = \rho^{(2)}$, respectively.

III. PERFORMANCE ANALYSIS

A. Outage Probability and Throughput

In this section, the performance of the proposed system considering throughput and outage probability metrics are investigated. The throughput of the system is calculated as

$$\tau^{(L,NL)(i)} = T(1 - P_{out}^{(L,NL)(i)})R^{th}/2, \quad (9)$$

where R^{th} denotes the target data rate of the system, and

$$P_{out}^{(L,NL)(i)} = Pr(\gamma_D^{(L,NL)(i)} < \gamma^{th}) = F_{\gamma_D}^{(L,NL)(i)}(\gamma^{th}), \quad (10)$$

and $\gamma^{th} = 2^{2R^{th}} - 1$. Here, γ^{th} indicates target threshold value. Considering (4), the CDF expression of γ_D for both L-EH and NL-EH models can be given as,

$$F_{\gamma_D}^{L(i)}(\gamma) = \int_0^\infty F_{\mathcal{V}^{(i)}}\left(\frac{\gamma}{u^{(i)}}\right) f_{\mathcal{U}^{(i)}}(u^{(i)}) du^{(i)} = 1 - \Delta_L^{(i)}, \quad (11)$$

and

$$\begin{aligned} F_{\gamma_D}^{NL(i)}(\gamma) &= P(\gamma < \gamma^{th} | \mathcal{U}^{(i)} < P_m)P(\mathcal{U}^{(i)} < P_m) \\ &\quad + P(\gamma < \gamma^{th} | \mathcal{U}^{(i)} > P_m)P(\mathcal{U}^{(i)} > P_m) \\ &= F_{\mathcal{U}^{(i)}}^{(i)}(P_m) + \Sigma^{(i)} \bar{F}_{\mathcal{U}^{(i)}}^{(i)}(P_m) \end{aligned} \quad (12)$$

where $P(\gamma < \gamma^{th} | Z < P_m) = 1$ and

$$\begin{aligned} \Sigma^{(i)} &= P(\mathcal{U}^{(i)} \mathcal{V}^{(i)} < \gamma, P_m < \mathcal{U}^{(i)} < P_{th}) \\ &\quad + P(P_{th} \mathcal{V}^{(i)} < \gamma, \mathcal{U}^{(i)} > P_{th}) \\ &= F_{\mathcal{U}^{(i)}}(P_{th}) - F_{\mathcal{U}^{(i)}}(P_m) - \Delta_{NL}^{(i)} \\ &\quad + F_{\mathcal{V}^{(i)}}(\gamma/P_{th}) \bar{F}_{\mathcal{U}^{(i)}}(P_{th}), \end{aligned} \quad (13)$$

respectively. Here, $u^{(i)} \in \{z, x\}$, $\mathcal{U}^{(i)} \in \{\mathcal{Z}, \mathcal{X}\}$, $v^{(i)} \in \{x, z\}$, and $\mathcal{V}^{(i)} \in \{\mathcal{X}, \mathcal{Z}\}$ for $i = \{1, 2\}$. Here for $i = 1$, (11) is given by substituting $f_{\mathcal{Z}}(z)$ and $F_{\mathcal{X}}(x)$ from (6) and (7), respectively. Moreover, for $i = 2$, (11) is given by substituting $f_{\mathcal{X}}(x)$ and $F_{\mathcal{Z}}(z)$ from (8) and (5), respectively. Furthermore,

$$\Delta_{\{\mathcal{L}^{(i)}, NL^{(i)}\}} = \int_a^b g(u^{(i)}) du^{(i)}, \quad (14)$$

where for $\Delta_L^{(i)}$ and $\Delta_{NL}^{(i)}$, the integral boundaries are set to $\{a = 0, b \rightarrow \infty\}$, and $\{a = P_m, b = P_{th}\}$, respectively. Here, $g(u^{(i)})$ can be given as,

$$g(u^{(i)}) = \bar{F}_{\mathcal{V}^{(i)}}(\gamma/u^{(i)}) f_{\mathcal{U}^{(i)}}(u^{(i)}). \quad (15)$$

1) *L-EH*: In this part, system performance of L-EH for both RIS-EH and RIS-IP cases are derived. It is clear to see from (4) that both proposed cases follow the same distribution ($\gamma_D^L = \mathcal{Z}\mathcal{X} = \mathcal{X}\mathcal{Z}$). Therefore, it is adequate to choose one of them, where we utilize $g(z)$ in (14) for both RIS-EH and RIS-IP cases. For both cases, substituting $f_{\mathcal{Z}}(z)$ and $F_{\mathcal{X}}(x)$ from (6) and (7), using [8, 01.03.26.0004.01], [8, 03.02.26.0067.01], and applying [7, 9.31-1] and [7, 9.31-2] in (15), we have (16), as shown at the bottom of the next page. Moreover, substituting (16) in (14) for $\{a = 0, b \rightarrow \infty\}$ and using [8, 07.34.21.0081.01], we can obtain (17), as shown at the bottom of the next page. Hence, substituting (17) in (11), the outage probability of the L-EH model is calculated for both cases where for RIS-EH case ($i = 1$), $\kappa = \varrho^{(1)}$, and $\varepsilon = v^{(1)}$ and for RIS-IP ($i = 2$), $\kappa = v^{(2)}$, and $\varepsilon = \varrho^{(2)}$. Please note that there is no built-in bivariate Meijer's-G function for this form of expression. Thus, we calculate numerical integral using (16) in (14) rather than closed-form equation

in (17). Finally, the throughput of the system is obtained by substituting (10) in (9).

2) *NL-EH*: Here, theoretical derivations of NL-EH model for both RIS-EH and RIS-IP cases are provided. As there is no-closed form expressions of $\Delta_{NL^{(i)}}$ in (14) for both RIS-EH ($i = 1$) and RIS-IP ($i = 2$) cases, we apply Gaussian-Chebyshev quadrature approach [12] to calculate (14) as

$$\Delta_{NL^{(i)}} = \int_{P_m}^{P_{th}} g(u^{(i)}) du^{(i)} = d_r \sum_{r=1}^{\rho} c_r \sqrt{1 - b_r^2} g(a_r) \quad (18)$$

where $a_r = 0.5((P_{th} - P_m)b_r + P_{th} + P_m)$, $b_r = \cos(\pi(2r - 1)/2\rho)$, $c_r = \pi/\rho$, $d_r = (P_{th} - P_m)/2$ and ρ denotes the trade off between complexity and accuracy. Substituting (5), (7), and (18) in (13), the outage probability of NL-EH model is calculated. Eventually, the throughput of the system is derived via substituting (10) in (9).

B. Average Harvested Power Analysis

In this part, the average harvested power of node S considering L-EH and NL-EH models for both EH-RIS, and EH-IP cases are calculated as

$$E^L[u^{(i)}] = \int_0^\infty u^{(i)} f_{\mathcal{U}^{(i)}}(u^{(i)}) du^{(i)}, \quad (19)$$

and

$$\begin{aligned} E^{NL}[u^{(i)}] &= E^{NL}[u^{(i)} | \mathcal{U}^{(i)} < P_m]P(\mathcal{U}^{(i)} < P_m) \\ &\quad + E^{NL}[u^{(i)} | \mathcal{U}^{(i)} > P_m]P(\mathcal{U}^{(i)} > P_m) \\ &= \bar{F}_{\mathcal{U}^{(i)}}(P_m)(\nabla_i(P_{th}) - \nabla_i(P_m) \\ &\quad + P_{th} \bar{F}_{\mathcal{U}^{(i)}}(P_{th})), \end{aligned} \quad (20)$$

respectively, where $E^{NL}[u^{(i)} | \mathcal{U}^{(i)} < P_m] = 0$. Here,

$$\nabla_i(\Pi) = \int_0^\Pi u^{(i)} f_{\mathcal{U}^{(i)}}(u^{(i)}) du^{(i)}, \quad (21)$$

and $\Pi = \{P_m, P_{th}\}$.

1) *L-EH*: Here, we present derivations of L-EH for RIS-EH and RIS-IP cases. Substituting $f_{\mathcal{Z}}(z)$, and $f_{\mathcal{X}}(x)$ from (6) and (8) in (19), the closed-form average harvested power for RIS-EH ($i = 1$) and RIS-IP ($i = 2$) cases are calculated as

$$E^L[z] = \frac{\alpha \varrho^{(1)} (2\sigma^2)^{2.25}}{2\mu} \exp\left(\frac{\mu^2}{4\sigma^2}\right) M_{-1.25, -0.25}\left(\frac{\mu^2}{2\sigma^2}\right), \quad (22)$$

and

$$E^L[x] = \varepsilon \Omega_w = \varrho^{(2)} \Omega_w, \quad (23)$$

respectively.

Here, (22), and (23) are calculated using [7, 6.6643-2], and [7, 3.326-10], respectively.

2) *NL-EH*: Here, closed-form solutions of NL-EH for both cases are covered. For the case RIS-EH ($i = 1$), utilizing [9, 2.3-31] and after some mathematical manipulation, the $f_{\mathcal{Z}}(z)$ in (6) is re-written as

$$f_{\mathcal{Z}}(z) = \alpha \lambda(k, \mu, \sigma^2, \varrho^{(1)}) z^{k-0.5} \exp\left(-\frac{z}{2\sigma^2 \varrho^{(1)}}\right), \quad (24)$$

where

$$\lambda(k, \mu, \sigma^2, \varrho^{(1)}) = \sum_{k=0}^{L_\lambda} \frac{(1/\varrho^{(1)})^{0.5+k}}{k! \Gamma(k+0.5)} \left(\frac{\mu}{2\sigma^2}\right)^{2k-0.5}, \quad (25)$$

and $L_\lambda = 200$. Substituting $f_{\mathcal{Z}}(z)$ from (24) in $\nabla_1(\Pi)$ in (21) and applying [8, 01.03.26.0004.01] with the aid of [7, 9.31-1]

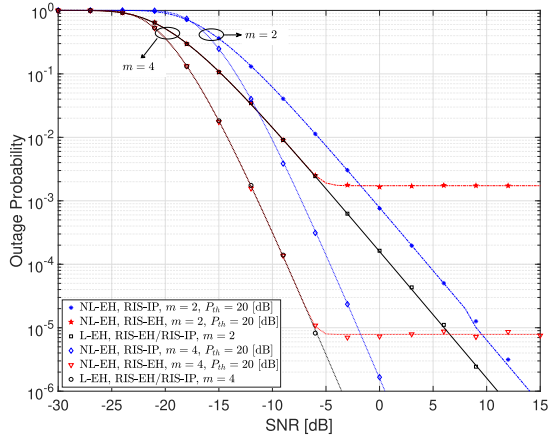


Fig. 2. Outage probability vs SNR of L/NL-EH models for $m = 2$ and $m = 4$ of RIS-EH/IP cases under $P_m = -20$ dB and $P_{th} = 20$ dB and $N = 30$.

and [7, 9.31-1], we have

$$\nabla_1(\Pi) = \alpha \lambda(k, \mu, \sigma^2, \varrho^{(1)}) \Pi^{k+1.5} \times G_{2,3}^{1,2} \left(\begin{matrix} -k-0.5, 1 \\ 0, 1, -k-1.5 \end{matrix} \middle| \frac{\Pi}{2\sigma^2\varrho^{(1)}} \right). \quad (26)$$

Here, (26) is calculated applying [8, 07.34.21.0003.01]. Finally, the NL-EH for RIS-EH is calculated by substituting (26) and $\bar{F}_{\mathcal{Z}}(P_{th})$ from (5) in (20).

For the case RIS-IP ($i = 2$), substituting $f_{\mathcal{X}}(x)$ from (8) in $\nabla_2(\Pi)$ in (21) and applying [7, 3.351-1] we have

$$\nabla_2(\Pi) = \varrho^{(2)} \Omega_w \gamma (m+1, m\Pi/\varrho^{(2)}\Omega_w) / (m\Gamma(m)). \quad (27)$$

The average harvested power of NL-EH for RIS-IP is calculated by substituting (27) and $\bar{F}_{\mathcal{X}}(P_{th})$ from (7) in (20).

IV. PERFORMANCE EVALUATION

In this section, we provide analytical results verified by numerical findings with Monte-Carlo simulations for the proposed RIS-empowered EH system. Unless, otherwise stated, energy conversation efficiency is set to $\eta = 0.5$, target data rate of the system is selected as $R^{th} = 1$, and node distances are selected as $d_{x,y} = d = 1$ [m] for $i \in \{1, 2, 3, 4, 5\}$ considering a path-loss exponent of $v = 2.7$.

In addition, we determine Nakagami- m parameters m_w, m_h and m_g are equally selected as m to ease of readability. Furthermore, we assume that $\rho = 200$, which ensures a reasonable trade-off between complexity and accuracy.

The outage probability of the proposed RIS-EH/IP cases is depicted with varying m parameters in Fig. 2 for L/NL-EH models. We also note that the end-to-end performance of the L-EH of the RIS-EH and RIS-IP provides the same

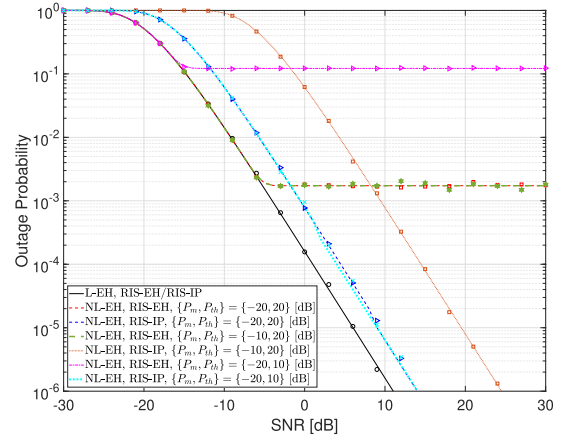


Fig. 3. Outage probability vs SNR of L/NL-EH models for varying P_m and P_{th} of RIS-EH/IP cases with $m = 2$ and $N = 30$.

outage probability performance due to the equal path-loss, as expected. Increasing m parameters brings diversity gain to both RIS-EH and RIS-IP. Applying $m = 4$ for RIS-EH/IP, approximately an SNR gain of 10 dB is obtained compared to $m = 2$ while providing an outage probability of 10^{-4} . However, in the NL-EH model, the system performance is limited due to the characteristics of the EH receiver circuit since the harvested power at S is saturated to P_{th} . In addition, the outage probability of the NL-EH model of the RIS-EH case goes to an error floor of approximately 10^{-3} and 10^{-5} , for both $m = 2$ and $m = 4$, respectively. Yet, it is observed that the RIS-IP case is not affected by P_{th} as much as RIS-EH since harvested power does not reach the threshold level.

Impact of P_m and P_{th} on outage probability performance of RIS-EH/IP cases is depicted in Fig. 3 for L/NL-EH models. It is observed that in the RIS-EH case P_m is not affected by outage probability performance since harvested power, obtained by RIS, is greater than P_m . For instance, at 10 dB SNR value, outage probability performance of the RIS-EH could be obtained as, approximately 10^{-3} for both $P_m = -20$ and $P_m = -10$. On the other hand, it is seen that the outage probability performance of the RIS-IP case does not go to the error floor since it does not reach P_{th} . However, in contrast to the RIS-EH case, P_m significantly impacts the outage performance of the RIS-IP case due to the sensitivity level of minimum transmission power. The throughput performance of the proposed system with respect to SNR is depicted in Fig 4. It is clear to observe that increasing P_{th} and N improves the throughput of the NL-EH model RIS-EH case significantly. An SNR gain of 10 dB for the RIS-EH case using L/NL-EH models is obtained by applying

$$g(z) = \pi \alpha \kappa^{-0.75} \sum_{t=0}^{m-1} \frac{1}{t!} \left(\frac{m\gamma}{\Omega_w \varepsilon} \right)^t z^{-t-0.25} G_{1,2}^{1,1} \left(\begin{matrix} 1 \\ 0, 1 \end{matrix} \middle| \frac{z}{2\kappa\sigma^2} \right) G_{2,1}^{1,1} \left(\begin{matrix} 1, 0 \\ 0 \end{matrix} \middle| \frac{\Omega_w \varepsilon z}{m\gamma} \right) G_{2,4}^{1,1} \left(\begin{matrix} 1, 0.25 \\ -0.25, 0.25, 0.25, 1 \end{matrix} \middle| \frac{z\mu^2}{4\kappa\sigma^4} \right) \quad (16)$$

$$\Delta_L = \pi \alpha \sum_{t=0}^{m-1} \frac{1}{t!} \left(\frac{m\gamma}{\Omega_w \varepsilon \kappa} \right)^t \left(\frac{1}{2\sigma^2} \right)^{t-0.75} G_{2,1:2,1:2,4}^{1,1:1,1:1,1} \left(\begin{matrix} t+0.25, t-0.75 \\ t-0.75 \end{matrix} \middle| \begin{matrix} 1, 0 \\ 0 \end{matrix} \middle| \begin{matrix} 1, 0.25 \\ -0.25, 0.25, 0.25, 1 \end{matrix} \middle| \frac{2\sigma^2 \Omega_w \varepsilon \kappa}{m\gamma}, \frac{\mu^2}{2\sigma^2} \right) \quad (17)$$

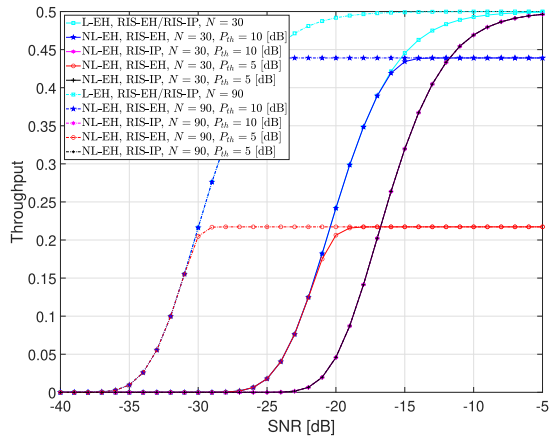


Fig. 4. Throughput of the RIS-EH/IP vs SNR for varied N and P_{th} values with $m = 2$, and $P_m = -20$ dB.

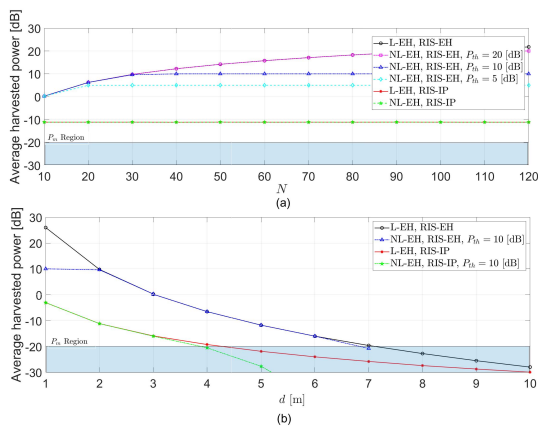


Fig. 5. Average harvested power of the proposed scenario for $m = 4$: a) Impact of N when SNR = 0 dB, $d = 1$ m, and $P_m = -20$ dB; (b) Impact of d when SNR = 0 dB, $N = 30$, $P_{th} = 10$ dB, and $P_m = -20$ dB.

$N = 90$ compared to $N = 30$. This implies that more elements increase the amount of harvested power in the L-EH model for the RIS-EH case. However, since harvested power is smaller than P_{th} , the throughput of both L/NL-EH models of RIS-IP provides the same results.

The impact of N and d on the average harvested power of the RIS-EH/IP cases are presented in Figs. 5 (a) and (b), respectively. According to the results of Fig. 5 (a) by improving N , the average harvested power for both the L/NL-EH models is increased in the RIS-EH case. However, the average harvested power saturates to their practical limited powers of $P_{th} = 5$ dB, $P_{th} = 10$, and $P_{th} = 20$ dB cases for $N > 20$, $N > 30$, and $N > 100$, respectively. RIS-IP is independent of the N value since RIS is located between S and D in this case. In addition, since the average harvested power of both L/NL-EH models are smaller than P_{th} , they provide the same result. Please note that L/NL-EH models and RIS-EH/IP satisfy sensitivity values and are higher than $P_m = -20$ dB. Moreover, according to the observations from Fig. 5 (b), the average harvested power versus d [m] is obtained. It is observed that in the RIS-EH case for $d > 2$ average harvested power is lower than $P_{th} = 10$. Consequently, average harvested power is equal for both L/NL-EH models. In the

RIS-IP case, both L/NL-EH are lower than P_{th} . Besides, the impact of P_m on the average harvested power NL-EH model could be seen for $d > 4$ [m] in the RIS-IP case.

V. CONCLUSION

In this letter, we have investigated the throughput, outage probability, and average harvested power for RIS-EH and RIS-IP based cases by deriving closed-form mathematical expressions, addressing both the L/NL-EH models. According to the results, the number of surface elements of RIS and the sensitivity/saturation power of the NL-EH model have a significant impact on the performance of the system. The L-EH model overestimates system performance and provides incorrect insight at high input power at the EH receiver. Meanwhile, the NL-EH model demonstrates a more practical system performance. In addition, the amount of harvested energy is directly proportional to the number of RIS elements in the RIS-EH case for the L/NL-EH models, yet it saturates to a predefined threshold power in the NL-EH model. Although the harvested energy of the RIS-IP is lower than the RIS-EH case, the performance of the RIS-IP links outperforms the RIS-EH case due to the existence of RIS between source and destination nodes. Consequently, RIS-IP is not as negatively impacted as RIS-EH in terms of threshold power for the NL-EH model. Finally, our theoretical analysis has been successfully validated by simulation results.

REFERENCES

- [1] N. Ashraf, S. A. Sheikh, S. A. Khan, I. Shaya, and M. Jalal, "Simultaneous wireless information and power transfer with cooperative relaying for next-generation wireless networks: A review," *IEEE Access*, vol. 9, pp. 71482–71504, 2021.
- [2] G. Zhou, C. Pan, H. Ren, K. Zhi, S. Hong, and K. K. Chai, "User cooperation for RIS-aided secure SWIPT MIMO systems under the passive eavesdropping," in *Proc. IEEE/CIC Int. Conf. Commun. China (ICCC Workshops)*, Jul. 2021, pp. 171–176.
- [3] L. Mohjazi, S. Muhaidat, Q. H. Abbasi, M. A. Imran, O. A. Dobre, and M. D. Renzo, "Battery recharging time models for reconfigurable intelligent surfaces-assisted wireless power transfer systems," *IEEE Trans. Green Commun. Netw.*, vol. 6, no. 2, pp. 1173–1185, Jun. 2022.
- [4] S. Lin, Y. Zou, J. Zhu, H. Guo, B. Li, and F. Xie, "Outage probability analysis of RIS-assisted wireless powered multi-user communications," in *Proc. 13th Int. Conf. Wireless Commun. Signal Process. (WCSP)*, Oct. 2021, pp. 1–5.
- [5] L. Zhao, Z. Wang, and X. Wang, "Wireless power transfer empowered by reconfigurable intelligent surfaces," *IEEE Syst. J.*, vol. 15, no. 2, pp. 2121–2124, Jun. 2021.
- [6] S. Dhok, P. Raut, P. K. Sharma, K. Singh, and C.-P. Li, "Non-linear energy harvesting in RIS-assisted URLLC networks for industry automation," *IEEE Trans. Commun.*, vol. 69, no. 11, pp. 7761–7774, Nov. 2021.
- [7] I. S. Gradshteyn, I. M. Ryzhik, and R. H. Romer, *Tables of Integrals, Series, and Products*. New York, NY, USA: Academic, 2014.
- [8] Wolfram. *The Wolfram Functions Site*. [Online]. Available: <http://functions.wolfram.com>
- [9] J. G. Proakis and M. Salehi, *Digital Communications*. New York, NY, USA: McGraw-Hill, 2008.
- [10] A. A. Nasir, X. Zhou, S. Durrani, and R. A. Kennedy, "Relaying protocols for wireless energy harvesting and information processing," *IEEE Trans. Wireless Commun.*, vol. 12, no. 7, pp. 3622–3636, Jul. 2013.
- [11] Y. A. Brychkov, "On some properties of the Marcum Q function," *Integral Transforms Special Functions*, vol. 23, no. 3, pp. 177–182, 2012.
- [12] Y. Ye, Y. Li, F. Zhou, N. Al-Dhahir, and H. Zhang, "Power splitting-based SWIPT with dual-hop DF relaying in the presence of a direct link," *IEEE Syst. J.*, vol. 13, no. 2, pp. 1316–1319, Jun. 2019.